A Quasi-Constant On-Time Control for SMPS With a Nonlinear Inductor Based on Power Switch Conduction Time Estimation

Daniele Scirè, *Member, IEEE*, Giuseppe Lullo, *Member, IEEE*, and Gianpaolo Vitale, *Senior Member, IEEE*

***Abstract*—This article proposes a control method for switching-mode power supplies equipped with nonlinear inductors; the method is based on the estimation of the conduction time (T_{ON}) of the power switch. The T_{ON} value is tuned according to the inductor model to obtain quasi-constant ON-time control. The method is devised for ferrite core power inductor, the nonlinearity is exploited up to saturation, condition where the differential inductance is reduced to half of its maximum value. This approach allows the calculation of the conduction time T_{ON} such that the maximum current of the inductor always corresponds to the saturation value while also considering the inductor temperature. This method obtains the current peak versus T_{ON} through a proper inductor model and a recursive algorithm for a given inductor temperature. The theoretical analysis was verified on a boost converter by comparing the simulations with experimental data with different loads, showing that the operating current can be increased by approximately 40% avoiding thermal runaway.**

***Index Terms*—Algorithm, inductors, nonlinear circuits, nonlinear estimation, saturable core, switched mode power supply (SMPS).**

NOMENCLATURE

$a_0, a_1, a_2, \ldots$	Coefficients of the polynomial form of the inductor current.
D	Duty cycle.
F_s	Switching frequency.
i_L	Current flowing through the inductor.
$\overline{i_L}$	DC current flowing through the inductor.
$i_{L,\max}$	Current peak of the inductor.
L	Inductance value.
$L_0, L_1, L_2, \ldots$	Coefficients of the inductance model.
L_{sat}	Inductance value at saturation.
L_{deepsat}	Inductance value in deep saturation.
LSR	Least square regression.
T_{core}	Temperature of the inductor.
T_{ON}	Conduction time of the power switch.
T_{OFF}	Blocking time of the power switch.
T_s	Switching period.
$\beta_0, \beta_1, \beta_2, \ldots$	Thermal coefficients of the inductor model.
ϵ	Convergence absolute tolerance.
Φ	Magnetic flux of the inductor.
Δi_L	Peak-to-peak current through the inductor in linear operation.
Δi_{L-nl}	Peak-to-peak current through the inductor in nonlinear operation.
v_L	Voltage across the inductor terminals.
V_s	Supply voltage.

Received 7 November 2022; revised 10 August 2024; accepted 2 October 2024. Paper no. TII-22-4601. *(Corresponding author: Daniele Scirè.)*

Daniele Scirè and Giuseppe Lullo are with the Department of Engineering, University of Palermo, 90128 Palermo, Italy (e-mail: daniele.scire@unipa.it; giuseppe.lullo@unipa.it).

Gianpaolo Vitale is with the Institute for high performance computing and networking, National Research Council (ICAR-CNR), 90146 Palermo, Italy (e-mail: gianpaolo.vitale@icar.cnr.it).

Color versions of one or more figures in this article are available at https://doi.org/10.1109/TII.2024.3477562.

Digital Object Identifier 10.1109/TII.2024.3477562

I. INTRODUCTION

OPTIMIZING the high power density in switching-mode power supplies (SMPS) is essential. Researchers have endeavored to address several aspects, such as improved topologies [1], new power-switching devices [2], electromagnetic interference filters [3], [4], advanced inductor modeling, and design techniques [5]. In addition, some papers dealing with new control techniques highlight the need for an accurate model of the converter components [6], [7], [8].

The power density of an SMPS can be improved by reducing the core of the inductor [4] and operating it beyond its linear region, up to saturation [9], [10], [11], [12]. The saturation zone is defined as the current at which differential inductance L_{sat} is reduced to half of its rated value. Beyond the linear region, the inductance value decreases and depends on both current and temperature. Here, the inductor exhibits nonlinear behavior; therefore, it is referred to as a nonlinear inductor. By exploiting saturation, a higher dc operating point can be set; however, reducing the inductance causes a higher current peak. Consequently, the power switch is more stressed and the losses increase [13].

This study focuses on the estimation of the current shape during the conduction time of the power switch (T_{ON}) because in a basic SMPS, it corresponds to the time interval in which the current through the inductor increases. Knowledge of this time interval is crucial because in a nonlinear inductor, the current

increases faster when approaching the end of the T_{ON}. For a fixed voltage across the inductor, the current derivative is inversely proportional to the inductance, which also depends on inductor temperature. Overestimation of the T_{ON} produces an overcurrent that can damage the power switch. Conversely, for a short T_{ON}, the operation occurs in the linear zone, nullifying the advantage of saturation exploitation.

Some studies dealing with constant ON-time control (COT) [14], [15] confirm the interest in this control technique; however, they can consider T_{ON} as a constant because the adopted inductor is linear. Calculating the T_{ON} for the conventional operation of an SMPS with a linear inductor is straightforward because it does not depend neither on the temperature of the inductor nor on its current. In contrast, when the inductor operates outside the linear zone, the behavior is nonlinear and the temperature must also be considered, emphasizing a dependence on the current. The novelty of this study is that an algorithm allows the tuning of the T_{ON} value based on temperature to obtain quasi-constant on-time control (QCOT).

In principle, the temperature can be retrieved using a suitable loss model [16]; however, knowledge of environmental temperature is required. The core temperature was measured using a thermocouple. In addition, the temperature distribution on the inductor is assessed and confirmed using thermal images.

The design of a QCOT requires suitable characterization and a proper model of the power inductor to describe the saturation [16]. The proposed recursive algorithm allows the calculation of the current peak based on T_{ON}, and vice versa. Starting from the maximum current imposed on the inductor and tuning the T_{ON}, it will always operate in saturation, avoiding thermal runaway regardless of the temperature. Although a practical application is discussed, the proposed method is general; it can be used to analyze the current through a nonlinear inductor when a constant voltage is applied for a given time interval.

The rest of this article is organized as follows. First, a short review of the models adopted for inductors in the literature is presented in Section II. Section III details the model adopted in this study. Section IV explains the characterization of the inductor used for experimental verification. Section V describes the main theoretical contribution, that is, the algorithm for the current estimation. Section VI proposes validation using a boost converter with two different loads, and the operations of the converter are based on the T_{ON} estimation according to core temperature. Section VII presents a discussion on the quality and the limitation of the proposed approach, paving the way for future developments. Finally, Section VIII concludes this article.

II. Review of the Inductor Modeling

The literature considers both the behavior of the inductor in saturation and the consequences of the SMPSs operation.

Analytical models, rather than physical models, are preferred for power electronics applications. Analytical models provide an external representation of the inductor using a relationship that gives the inductance versus current (with temperature as a parameter). Many approaches use general and well-known modeling techniques; two of them are based on a function that shows a shape similar to the inductance variation to be reproduced, such as the arctangent [9] and polynomial models [17].

Considerable attention has been paid to ferrite as a core material owing to its low losses over a wide frequency range and high specific resistivity [18]. However, ferrite exhibits an abrupt decrease in the inductance when saturation is achieved [10], [19], [20].

Several analytical models have been proposed that show different tradeoffs between the accuracy and calculation resources. The improved arctangent-based method [12] provides good accuracy for the entire inductor curve, including the temperature variations. Such a model can be implemented in a simulation to reliably reproduce the current waveform in a dc–dc converter at the operating temperature [21]. The piecewise-affine formulation [22] improves the use of the computational resources of Oliveri et al. [12]. Hammerstein modeling can also provide nonlinear functions in power electronics, as in [23], where it is applied to characterize different ferrite inductors using a pulse compression identification technique. In [24], a neural network model (E-αNet) was developed to reproduce the ferrite power inductors inductor behavior up to saturation also considering the core temperature. The so-called local approach generally adopts different approximations depending on the current. The main disadvantage is the discontinuity of the inductance curve, which can only be used for small current variations [11]. The solution proposed in this article takes advantage of a polynomial model that approximates the inductance variation, including temperature dependence [25]. The inductor temperature can be considered constant during the switching period. Therefore, a model of the inductor at a given temperature is suitable for reproducing the current waveform when the temperature is known. However, during operation, the inductor modifies its behavior owing to a thermal transient, whose duration is of the order of tens of seconds; consequently, the inductance variation versus temperature has been considered. This implies that different core temperatures require different T_{ON} values to exploit saturation, whereas all the other parameters remain unchanged. The devised QCOT is useful since it varies the switching frequency, maintaining the duty cycle imposed by the converter control, always assuring a proper T_{ON} value. The goodness of the model consists of reproducing the current profile under operating conditions, including the temperature increase due to losses [21], [26] and dangerous operations, potentially causing thermal runaway [16], [27], [28], [29], [30].

III. Inductor Modeling by Polynomial

The proposed approach considers an inductor modeled using a polynomial function. This model was successfully applied to the behavior of saturable reactors in [25]; here, it was adapted to ferrite power inductors, including temperature [16], [31]. It reproduced the sharp transition from linear to saturation, and proved to be computationally lightweight, providing a good approximation with a third-order polynomial [16], [17]. In contrast to saturable reactors operated in ac, the power inductors used in SMPSs operate with a dc offset and superimposed ac signal; therefore, a different characterization system is required [32].

TABLE I
MODEL COEFFICIENT OF THE INDUCTOR

Coefficient	Value	Coefficient	Value
L_0	384.7 μH	β_0	−0.002815 °C^{-1}
L_1	−214.2 μH/A	β_1	−0.02464 °C^{-1}
L_2	312.6 μH/A^2	β_2	−0.02034 °C^{-1}
L_3	−110.1 μH/A^3	β_3	−0.01335 °C^{-1}
L_{deepsat}	70.0 μH		

The polynomial coefficients are considered to be linearly dependent on the temperature, implying that the magnetic flux increases linearly with temperature for a given magnetizing current. The characterization of the work in [33] in terms of the saturation flux shows that a linear trend can approximate it for the temperature range 25–125 °C. Moreover, we experimentally verified this behavior in the studied inductor.

The inductance is modeled as

$$L(i_L, T_{\text{core}}) = \begin{cases} \sum_{m=0}^{3} L_m(1+\beta_m T_{\text{core}}) i_L^m, & L(i_L) > L_{\text{deepsat}} \\ L_{\text{deepsat}}, & \text{otherwise} \end{cases} \quad (1)$$

where L_m are polynomial coefficients, and the linear dependence of the inductor temperature T_{core} (°C) is expressed by the proportionality factors β_m. The parameter L_{deepsat} is the inductance value when deep saturation (also known as hard saturation) is reached, where the flux density is almost constant. The first term in (1) corresponds to the thermal behavior of a traditional linear inductor. Once the coefficients are known, (1) can be easily implemented and requires minimal computational resources. However, the coefficients L_m, β_m, and L_{deepsat} need to be previously identified; they were obtained experimentally using the method explained in Section IV. Once the model is identified, the practical limit or saturation point (L_{sat}), where the differential inductance is halved, can be retrieved.

IV. INDUCTOR CHARACTERIZATION

The main issues related to inductor model identification for linear inductors are discussed in [34]. However, as explained above, a nonlinear inductor requires a different characterization method. This was performed using the test system described in [32] and [35] to obtain a representation of the inductor as in (1).

The operating principle of the characterization system can be summarized as follows. The inductor under test was inserted into a dc/dc converter with a variable active load. It is automatically controlled by a LabVIEW-based instrument that imposes 1) the switching frequency, 2) the duty cycle of the power switch, 3) the dc bias current by varying the load value, and 4) the inductance L, which is calculated by the ratio between the voltage applied to the inductor (maintained constant) and the slope of the current.

The measurement system was applied to a 330 μH inductor delivered by a Coilcraft model DO-5010H-334. The identified coefficients corresponding to (1) are given in Table I, and their characteristic curves are shown in Fig. 1, considering the temperature. For low currents, the inductance is constant, and the temperature does not affect this value, which corresponds to a linear inductor operation. By increasing the current, the inductance

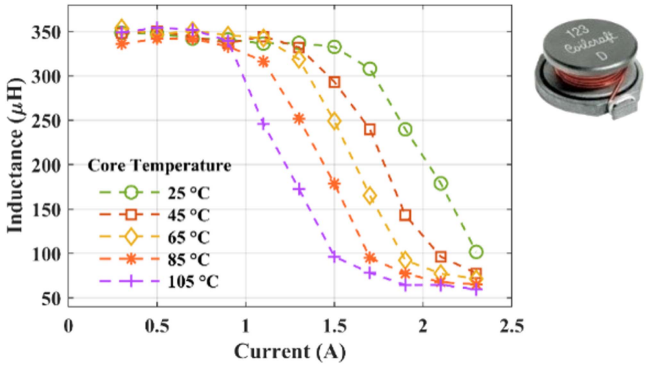

Fig. 1. Inductance versus current versus core temperature of the Coilcraft 5010H-334.

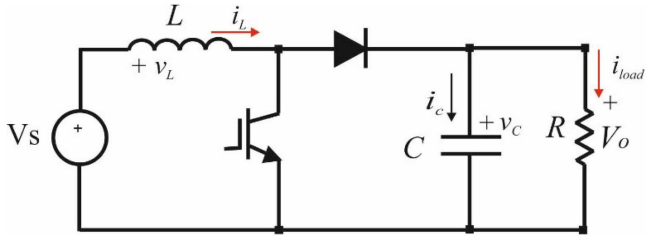

Fig. 2. Electrical scheme of a boost converter.

varies with temperature, resulting in different current curves. It should be remarked that, from the characteristic curves shown in Fig. 1, the use of the Coilcraft 5010H-334 inductor in linear zone can be performed with a current up to 1 A. Instead, by nonlinear operation, the operating point can be increased by 40%, meaning a current of 1.4 A with a temperature core of 85 °C. At this point, the rated inductance is reduced to approximately 200 μH. The same current with linear operation would require a larger core inductor, such as 5040H-330, which exhibits a larger volume of approximately 70%. This demonstrates that a design with a nonlinear inductor improves power density. An increase of 40% in the rated current can be assumed as a safe tradeoff between limiting the nonlinear operations and achieving a high-density SMPS design and can be considered as a practical target by the designer.

V. ESTIMATION OF THE MAXIMUM CONDUCTION TIME AND CURRENT PEAK

After the inductor characterization, there is need to calculate its current when it is operated in a converter. The inductor current estimation is performed considering a boost converter as a case study; the analysis can be extended to other SMPS without losing generality because the inductor is supplied by a constant voltage for a given time interval as in basic dc/dc converters and in many other topologies. The time interval depends on the switching frequency and the duty cycle. The voltage and time intervals were chosen based on the converter.

In a boost converter (see Fig. 2) with a linear inductor operated in a continuous current mode, the current flowing through the

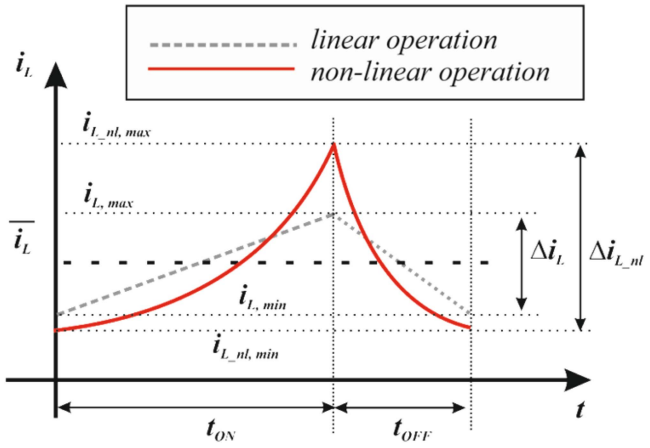

Fig. 3. Comparison of current waveforms with linear and nonlinear inductors.

inductor exhibits a triangular shape, and the current variation can be easily calculated. Instead, when the inductor is exploited outside the linear region, the current differs from the well-known triangular waveform and its time derivative increases with time.

Fig. 3 compares the current waveforms for linear and saturated inductors with the same average current. The mean value $\overline{i_L}$ of the current does not vary because it depends on the load (neglecting losses in first approximation); consequently, the two areas defined by the nonlinear curve under and over the mean value $\overline{i_L}$ must be the same. Instead, because of the upward concavity of the current waveform for the nonlinear inductor, the current peak $i_{L-nl,\max}$ increases, and the current variation in the nonlinear case Δi_{L-nl} is higher than the value in the linear case Δi_L.

The following section presents an analysis of the nonlinear inductor. If the inductance is not constant, the general relationship between inductor voltage v_L and flux Φ must be considered

$$v_L(t) = \frac{\delta\Phi(i_L, T_{\text{core}})}{\delta t} \tag{2}$$

where T_{core} is the core temperature, which is practically constant during the switching period.

Equation (2) can be expanded as

$$v_L(t) = \frac{d\Phi(i_L)}{di_L} \cdot \frac{di_L(t)}{dt} = L(i_L)\frac{di_L(t)}{dt} \tag{3}$$

where inductance is considered a polynomial function of the current, as in our case, using (1). Equation (3) can be solved numerically in a time interval equal to the T_{ON}, where v_L is a constant

$$i_L(k+1) = i_L(k) + \frac{v_L \Delta t}{L(i_L(k))}. \tag{4}$$

Discretization (4) follows the Euler method to simplify the description. However, the fourth-order Runge–Kutta method was used in our simulations to achieve a better accuracy. Equation (4) requires n steps corresponding to $n+1$ points from $t=0$ to T_{ON}, with $\Delta t = T_{\text{ON}}/n$. The starting value is $i_L(0)$, that is, the minimum value of the current $i_{L,\min}$.

Initially, (4) is solved, starting with $i_{L,\min} = 0$ for a time interval equal to T_{ON}, thus generating a vector containing n samples of the current. Next, the current samples were fitted with a polynomial function of time using the coefficients a_j

$$i_L(t) = a_0 + a_1 \cdot t + a_2 \cdot t^2 + \cdots + a_5 \cdot t^5. \tag{5}$$

In this study, a fifth-order polynomial for (5) was used to achieve a reasonable accuracy. To retrieve an interpolating polynomial curve, an LSR is applied to the discrete waveform obtained by (4) such that the coefficients a_j of (5) can be found. The LSR can be applied because the error in the measured time is much lower than the error in the current measurement, which follows the Gauss theorem because it is retrieved experimentally, and all events are independent (no memory effect occurs) with the same variance.

To perform LSR, (5) is written in a matrix form as follows: matrix $\boldsymbol{A}$ has as many columns as the number of coefficients to be identified (corresponding to the degree of the polynomial plus one) and a number of rows equal to $n = T_{\text{ON}}/\Delta t$. Each row contains the time raised to the power corresponding to the coefficient of the current

$$\boldsymbol{A} = \begin{bmatrix} 1 & 0 & \dots & 0 \\ 1 & \Delta t & \dots & \Delta t^m \\ \vdots & \vdots & \ddots & \vdots \\ 1 & T_{\text{ON}} & \dots & T_{\text{ON}}^m \end{bmatrix} \boldsymbol{p} = \begin{bmatrix} a_0 \\ a_1 \\ \vdots \\ a_m \end{bmatrix} \boldsymbol{y} = \begin{bmatrix} i_L(0) \\ i_L(\Delta t) \\ \vdots \\ i_L(T_{\text{ON}}) \end{bmatrix}. \tag{6}$$

Due to the error distribution, a solution as $\boldsymbol{y}^T = \boldsymbol{p} \cdot \boldsymbol{A} + \boldsymbol{e}$ can be obtained, where $\boldsymbol{e}$ denotes an error vector. Under the hypothesis of a normal distribution of the error and null mean, the Gauss Markov theorem gives the solution vector of coefficients as

$$\boldsymbol{p} = \left(\boldsymbol{A}^T \boldsymbol{A}\right)^{-1} \boldsymbol{A}^T \boldsymbol{y}. \tag{7}$$

The coefficients a_j must satisfy the following condition:

$$\overline{i_L} = \frac{1}{T_{\text{ON}}} \int_0^{T_{\text{ON}}} i_L(t)dt. \tag{8}$$

The value $\overline{i_L}$ is the dc current through the inductor. This is imposed by the load. By substituting (5) into (8), the mean value of the current is given by

$$\overline{i_L} = a_0 + \frac{1}{2}a_1 \cdot T_{\text{ON}} + \frac{1}{3}a_2 \cdot T_{\text{ON}}^2 + \cdots + \frac{1}{6}a_5 \cdot T_{\text{ON}}^5. \tag{9}$$

From (5), it can be noted that coefficient a_0 represents the minimum value of the current $i_{L,\min}$ obtained for $t=0$.

Once interpolation was performed, it was possible to invert (9) to calculate a new value of a_0. By substituting a_0 in (4) as a new starting point $i'_{L,\min}$, the procedure can be repeated until convergence is obtained, that is, when the difference between the new starting point and the previous starting point is less than the tolerance ϵ. In the discontinuous current mode operation of the SMPS, iterations are unnecessary because the value of $i_{L,\min}$ is always null.

Algorithm 1: Estimation Algorithm for Calculating $i_{L,\max}$ and $i_{L,\min}$.

$i_{L,min} \leftarrow 0$ ▷Initialize with a zero-initial current
$i_L(0) \leftarrow i_{L,min}$ ▷Set the initial current $i(0)$
repeat
  for $k \leftarrow \{0, \ldots, n-1\}$ ▷n steps are required for calculation of (4)
    $L = L_0(1+\beta_0 T_{core}) + L_1(1+\beta_1 T_{core}) i(k) + \ldots$ ▷Inductance calculation (1)
    if $L < L_{deepsat}$ ▷Inductance saturation evaluation
      $L \leftarrow L_{deepsat}$ ▷Inductance set to the saturation value (1)
    end if
    $i_L(k+1) \leftarrow i_L(k) + v_L \Delta t / L$ ▷Step for calculation of (4)
  end for
  $\overline{i_L} = \frac{1}{T_{ON}} \int_0^{T_{ON}} i_L(t)dt$ ▷Mean current evaluation (8)
  LSR algorithm ▷Algorithm for the a_j evaluation
  $i_L(0) \leftarrow a_0$ ▷Set the initial current $i_L(0)$
until $|i'_{L,min} - i_{L,min}| < \epsilon$ ▷Repeat the process until tolerance ϵ is reached
$i_{L,max} = a_0 + a_1 \cdot T_{ON} + a_2 \cdot T_{ON}^2 + \ldots$ ▷Maximum current evaluation (10)

After convergence, the curve that reproduces the current is identified using polynomial (5). The maximum current value can be obtained by (5) and evaluated for $t = T_{\text{ON}}$

$$i_{L,\max} = a_0 + a_1 \cdot T_{\text{ON}} + a_2 \cdot T_{\text{ON}}^2 + \cdots + a_5 \cdot T_{\text{ON}}^5. \quad (10)$$

The calculation method explained here is concisely schematized in Algorithm 1. It provides the peak current ($i_{L,\max}$) through an inductor for a given T_{ON}.

Therefore, the evaluation of the maximum current was repeated by applying Algorithm 1 to the different core temperatures. Each iteration yields a triplet of $i_{L,\max}$, T_{ON}, and T_{core}. Considering that this study aims to derive the maximum allowed conduction time for a fixed maximum current, the dataset of the collected triplets can be arranged in a lookup table (LUT). Complementary, the dataset can be used to obtain the regression f and the relationship between the maximum conduction time, peak current, and core temperature as in (11). In the practical implementation, it allows retrieving the T_{ON} based on the measured temperature and the maximum current imposed to the inductor

$$T_{\text{ON,max}} = f\left(i_{L,\max}, T_{\text{core}}\right). \quad (11)$$

VI. Validation

A. Boost Converter and Measurement Setup Description

The boost converter used for the validation test was supplied with $V_s = 24$ V. It adopts an FDP12N60NZ MOSFET as the switch, and an STTH806 rectifier as the diode. The component selection was driven by the need for a reliable and available prototype setup with a significant safety margin, but also flexible in order to leave the possibility to scale-up the power rating in future works. The operation of the control system is illustrated in the block diagram, as shown in Fig. 4. The QCOT module is drawn by gray lines; it represents an add-on compatible with the existing control. The prototype is shown in Fig. 5(a). The inductor under test was a ferrite core inductor (Coilcraft DO-5010H-334, L_{NOMINAL} 330 μH). This component is characterized as explained in Section IV. A UT70B digital multimeter from Lafayette equipped with a K-type thermocouple (range of $-40 \div 260$ °C; accuracy of $\pm 0.75\%$) is used to measure the core temperature of the inductor. The temperature distribution of the inductor [see Fig. 5(b)] was measured through thermal imaging using a camera model FLIR SC660; its temperature measurement capability ranges from -40 to 1500 °C with 1 °C accuracy. For better visualization in each thermal image, the color palette was started at room temperature and ended at the highest temperature of each measurement. The thermal analysis verifies that during operation, 1) the temperature of the core is not influenced by the heatsink of the MOSFET, and 2) the temperature measurements made with a thermocouple in contact with the coil core are coherent with thermal imaging.

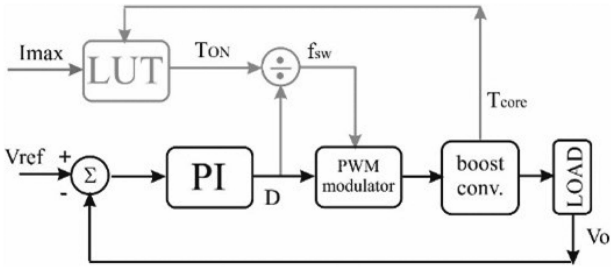

Fig. 4. Proposed block diagram of the control system.

The classical pulsewidth modulation (PWM) control loop is updated with information from the LUT, providing the T_{ON} based on both the maximum current peak imposed on the inductor and the core temperature. The switching frequency in the PWM modulator was calculated from the T_{ON} and required duty cycle. The entire test rig is shown in Fig. 5(c). The photograph and the thermal images have been performed removing the converter box only for the time needed to take the picture. In the following, three situations are described.

1) Operation of the converter in an open loop with a constant T_{ON}, to show how the current peak increases as the temperature of the inductor increases.
2) Starting from the same operating point of the last test, an operation with the proposed QCOT, showing that the current peak remains constant owing to the control system, which avoids thermal runaway.
3) An example of the thermal runaway due to the excessive mean inductor's current.

B. Operation With Constant T_{ON}

The main waveforms of the boost converter operated with a constant T_{ON} and switching frequency of 46 kHz are shown in Fig. 6(a) for different core temperatures. This shows the evolution of temperature during operation in an open loop. Fig. 6(b)

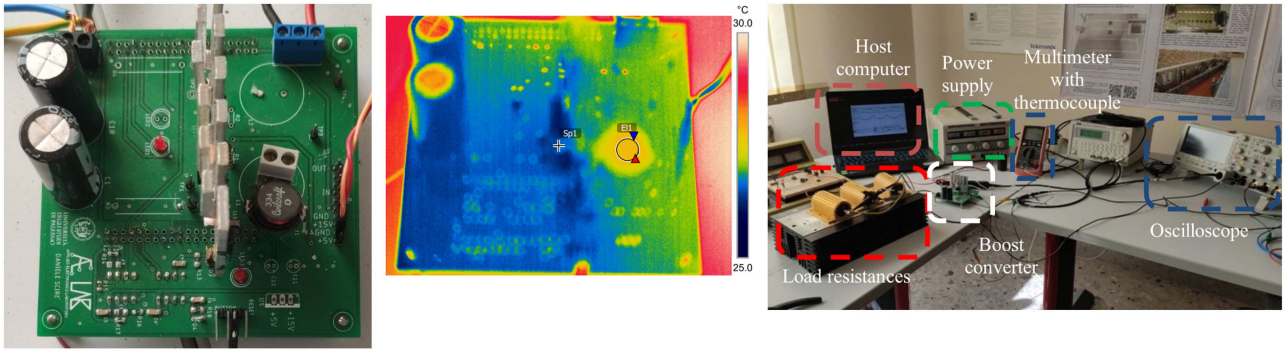

(a) (b) (c)

Fig. 5. (a) Prototype of the boost converter used for test. The free-wheel diode is mounted on the backside of the PCB. (b) Thermal image of the converter in standby. (c) Photograph of the test rig.

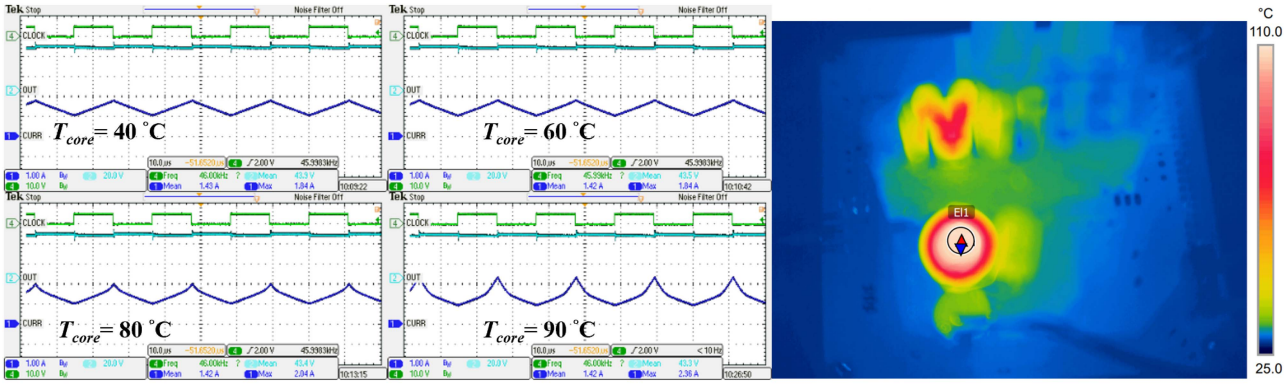

(a) (b)

Fig. 6. (a) Example of an open-loop thermal runaway: duty cycle (top), output voltage (middle), and current through the inductor (bottom) of the boost converter increasing the temperature at a constant frequency of 46 kHz corresponding to a fixed T_{ON} of 10.9 μs. The mean current is 1.4A. (b) Thermal image of the converter when the inductor reaches the temperature of 105 °C.

shows thermal images obtained at the highest temperature. The converter starts at environmental temperature (25 °C), and during operation, it reaches 105 °C. At $T_{\text{core}} = 60$ °C, the inductor is still in linear operation; after 150 s, its temperature is equal to 80 °C, and an increase in the current peak can be observed. This increase is further evident after 813 s ($T_{\text{core}} = 105$ °C). Photographs and thermal images were obtained by removing the converter box only for the time required to capture the images. It should be noted that an increase in the temperature modifies the current waveform. The power inductor operates in the linear zone only at low temperatures and exhibits a well-known triangular shape. Subsequently, the temperature increase drives it toward saturation, with a consequent increase in the current peak. It demonstrates that a constant T_{ON} operation cannot ensure safe operation in saturation because the current peak depends on the temperature. It assesses the need to estimate T_{ON} versus temperature. Finally, it is worth noting that the traditional voltage closed-loop feedback worsens the thermal runaway, which is inherently unstable. This increases the duty cycle to maintain a constant output voltage against losses. Consequently, the current peak further increases, increasing the losses and, therefore, the temperature, thus generating the thermal runaway.

C. Operation With QCOT Technique

By applying Algorithm 1, triplets ($i_{L,\max}$, T_{ON}, and T_{core}) were retrieved for a specific mean current of the inductor corresponding to a given load value and output voltage. Two case studies were presented by choosing an output voltage of 48 V and two different mean inductor current values (1.4 and 1.9 A) obtained with two loads of 63 and 50 Ω, respectively. Fig. 7 depicts a 3-D representation of the triplets ($i_{L,\max}$, T_{ON}, and T_{core}) obtained by running Algorithm 1 when the load is 63 Ω. It can be noted that for high temperature and conduction time, the maximum achievable current highly exceeds the rating current of the inductor, limiting, therefore, the operating region of the converter. However, reducing either the temperature or the conduction time reduces the current peak to a safer value.

Fig. 8 presents the current peak as a function of conduction time, which was parameterized to the core temperature. It is

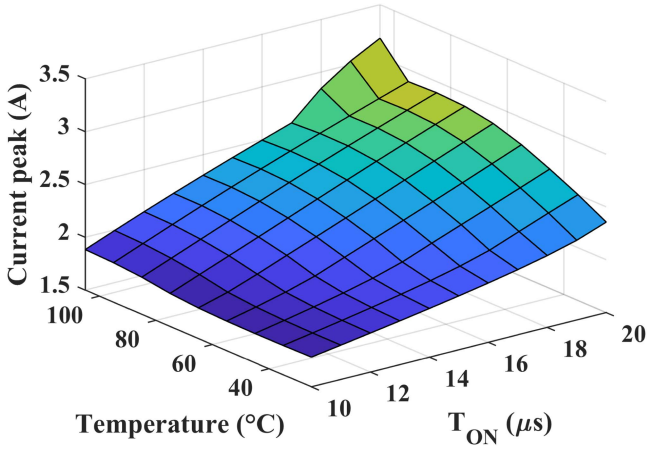

Fig. 7. Surfaces representing maximum current peak versus core temperature versus conduction time obtained for the 63 Ω load.

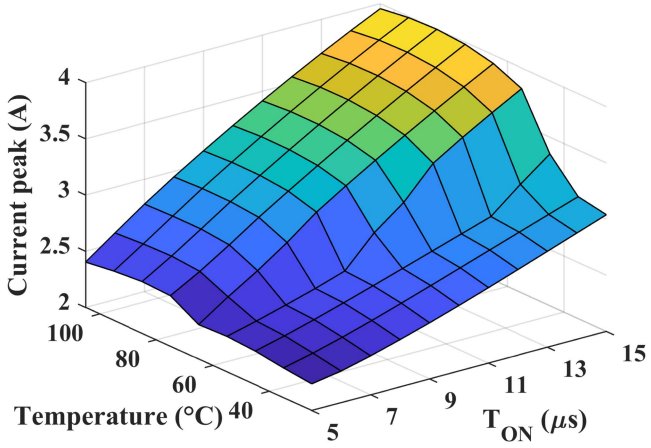

Fig. 9. Surfaces representing maximum current peak versus core temperature versus conduction time obtained for the 50 Ω load.

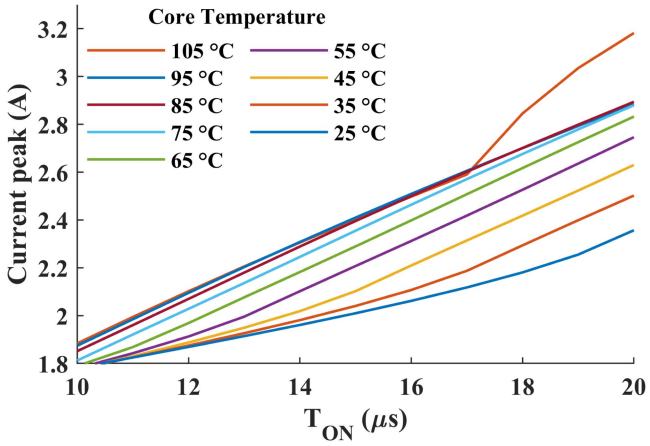

Fig. 8. Relationship between peak current and the conduction time for different core temperatures obtained for the 63 Ω load.

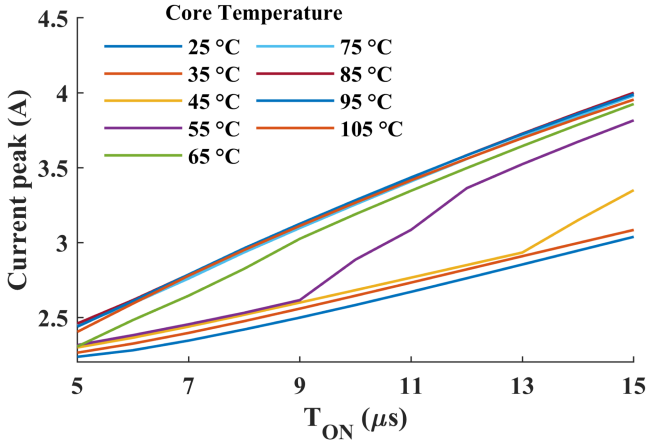

Fig. 10. Relationship between peak current and the conduction time for different core temperatures obtained for the 50 Ω load.

worth noting that the current peak presents a linear trend as a function of the conduction time (see Fig. 9), except when the core temperature and high conduction time bring the inductor to deep saturation. In the latter case, the current slope versus conduction time increased, rapidly increasing the current peak. Similar results are shown in Fig. 10 for the case study with a load of 50 Ω, where the converter has a smaller region in which the current peak is below the maximum rated inductor current. It is worth noting that for the highest and lowest temperatures, the maximum current exhibited a linear trend as a function of the conduction time. Instead, for intermediate temperatures (e.g., 45 and 55 °C), the slope increased after exceeding a specific conduction time.

The two case studies were first simulated to address an adequate load value, and then implemented on the boost converter previously described to validate the proposed method. The simulation resulted in LUTs being used to set the conduction time. The first case is presented in Fig. 11(a) (load of 63 Ω corresponding to a mean inductor current of 1.4 A with a 40% increase to the rated value), where the inductor saturation is correctly exploited, and the temperature stabilizes at about 90 °C [see Fig. 11(b)]. The maximum current peak was set to 1.8 A and the current waveform was not linear for temperatures higher than 60 °C. The control system regulates the output voltage (operational safety is assured by T_{ON} control) by varying the switching frequency in the range of 46–74 kHz. For the chosen $i_{L,max}$, an appropriate conduction time is set based on the measured inductor temperature (see Fig. 8). Similar results were obtained in another case study (see Fig. 12) with an output load of 50 Ω, corresponding to an inductor mean current of 1.9 A. In this case, the current peak was set to a higher value (2.6 A), overcoming saturation, and the conduction time regulation was obtained by varying the switching frequency in a broader range of 40–105 kHz. Although the current peak was maintained constant, a temperature runaway was experienced, and the measurements were stopped to prevent any damage to the converter after the safe temperature threshold was reached at 105 °C. From the tests reported above, it can be deduced that, by using an inductor up to saturation to reduce its core size in an SMPS, the T_{ON} time of the power switch must be tuned during operation to

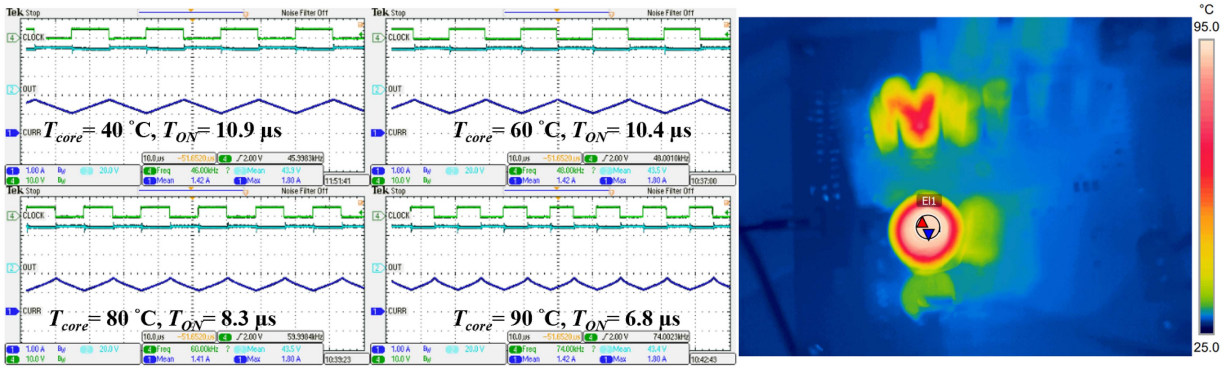

Fig. 11. (a) Example of stable operation exploiting nonlinearity: duty cycle (top), output voltage (middle), and current through the inductor (bottom) of the boost converter with variable T_{ON} and frequency as the temperature rises. It can be noted that the peak current remains constant despite the temperature variation because the ON time is reduced by the control system. The temperature stabilizes at about 90 °C after about 7 min from startup. (b) Thermal image of the converter when the inductor reaches the temperature of 90 °C.

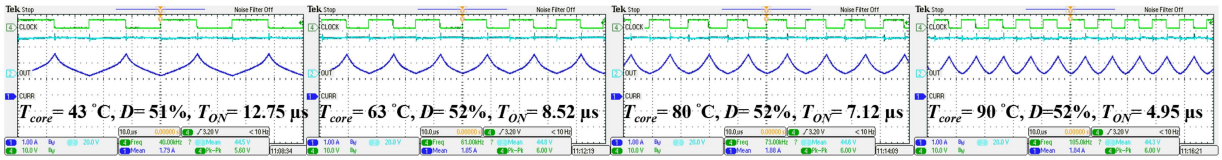

Fig. 12. Example of thermal runaway due to the excessive mean current: duty cycle (top), output voltage (middle), and current through the inductor (bottom) of the boost converter with variable T_{ON} and frequency as the temperature rises. It can be noted that the peak current remains constant despite the temperature variation because the ON time is reduced by the control system. The temperature is not stable and exceed 105 °C, therefore, the measurement was stopped to prevent any damage.

ensure that the current has a constant peak value. Therefore, the constant T_{ON} technique was modified into a QCOT technique. This implies a frequency variation whose range depends on the load value. The higher the load current, the wider the frequency variation interval. The QCOT ensures stable operation with an increase of up to 40% in the inductor mean current with respect to the maximum allowed by the manufacturer. The power switch is commutated at the end of the T_{ON}, without the need for a dedicated circuit for current-threshold detection. Even if the proposed approach requires temperature measurement, the related circuit is simpler than the current detection and does not require fast intervention because the thermal evolution of the inductor is slow and can take tens of seconds. Furthermore, the temperature measurement prevents a thermal runaway. Finally, it can be observed that the proposed QCOT allows a higher mean current through the inductor (up to 40%), which can be chosen with a smaller core compared to a linear operation. In our case, the volume of the inductor was reduced by 70% compared with that of the 5040H-330 inductor that operates in the linear zone.

VII. Discussion and Future Outlook

The aim of this article is to demonstrate the feasibility of using saturable inductors in SMPS applications, highlighting the potential benefits in terms of inductor size reduction. The adaptive ON time control based on the thermal model of the inductor is implemented as an effective strategy to prevent thermal runaway caused by saturation. This feasibility has been assessed by a low-voltage, low-power dc–dc boost converter with a switching frequency ranging from 40 to 105 kHz. This converter has been initially conceived to test and characterize nonlinear inductors based on LabVIEW. Then, we devised the QCOT control as an add-on requiring low computational resources (represented by gray color in Fig. 4). In this way, the dynamics of the system is always governed by the PI controller that imposes the duty cycle whereas the QCOT manages the switching frequency for given temperature. The QCOT module introduces a negligible delay since it requires reading the LUT and a division. The adopted setup has the following limits: it uses a relatively high 330 μH inductance, the maximum switching frequency is limited by the MOSFET conduction resistance and by the LabView implementation. On the other hand, this experimental setup assesses using a smaller and lighter SMPS through the exploitation of inductors up to the saturation point. A modern implementation would benefit of higher switching frequencies allowing for smaller inductances and of the use of a low-cost microcontroller for the QCOT algorithm implementation, e.g., the TMS320F28379D from Texas Instrument (clock frequency up to 200 MHz), allowing for the implementation of the QCOT at much higher switching frequency with the use of smaller inductors.

The proposed QCOT has been tested with a constant input voltage; however, the variable input can be managed by a family of LUTs calculated in the expected range of input voltages. For a given input voltage, the corresponding LUT is selected.

With the implementation of the LUT family, the QCOT can address significant variations in input voltage, which is of particular interest in applications, such as LED drivers and automotive

systems, where large voltage surges are common. Indeed, in case of SMPS exploiting nonlinear inductors, also the maximum input current must be regulated by the QCOT to avoid the deep saturation of the inductor core.

On this basis, for any given inductor, its operating range can be extended up to the 40% of the rated current, the proposed characterization allows defining the operating frequency range; the constraint for the choice of the microprocessor is represented by the maximum switching frequency for the PWM modulator. Once the inductor characterization is performed offline, the implementation as an add-on is simple.

VIII. Conclusion

The exploitation of the nonlinearity of a power inductor up to the saturation zone in SMPSs requires that the conduction time of the power switch is tuned based on the inductor behavior, which depends on both current and temperature. However, it allows a current threshold higher than that of a linear inductor with the same rated value, but with a reduced volume, thus improving the power density.

This article proposes a method for retrieving the current flowing through a nonlinear inductor that operates up to saturation.

This method was exploited by an algorithm to estimate the time required for the current to reach the maximum value corresponding to the conduction time of the power switch. It is a recursive algorithm from which a complete characterization of the inductor in terms of T_{ON} versus current peak and versus core temperature is obtained. These curves, which were implemented in a LUT, were used to implement a quasi constant T_{ON} technique in the boost converter. The QCOT implementation is an add-on tool that preserves the dynamic of the PI control and imposes the switching frequency maintaining the duty cycle. Two case studies were proposed with two different loads to demonstrate that an increase of 40% in the rated current corresponding to saturation exploitation can be managed by the QCOT algorithm. The QCOT increased the switching frequency to tune a suitable T_{ON} value. A current exceeding saturation leads to thermal runaway, which is stopped by temperature detection. The increase in the operating current of 40% resulted in a 70% reduction in the volume and a cheaper inductor.

Acknowledgment

The authors would like to thank the technicians of ICAR-CNR Giampiero Rizzo for their support in setting up the computational system to carry out the simulations and Giovanni Ruggieri to arrange the hardware to perform the experimental test given in this article.

References

[1] N. Lee, J.-Y. Lee, Y.-J. Cheon, S.-K. Han, and G.-W. Moon, "A high-power-density converter with a continuous input current waveform for satellite power applications," *IEEE Trans. Ind. Electron.*, vol. 67, no. 2, pp. 1024–1035, Feb. 2020.

[2] D. Shahzad, S. Pervaiz, N. A. Zaffar, and K. K. Afridi, "GaN-based high-power-density AC–DC–AC converter for single-phase transformerless online uninterruptible power supply," *IEEE Trans. Power Electron.*, vol. 36, no. 12, pp. 13968–13984, Dec. 2021.

[3] M. L. Heldwein and J. W. Kolar, "Impact of EMC filters on the power density of modern three-phase PWM converters," *IEEE Trans. Power Electron.*, vol. 24, no. 6, pp. 1577–1588, Jun. 2009.

[4] D. Scirè, G. Lullo, and G. Vitale, "EMI filter re-design in a SMPS with inductor in saturation," in *Proc. IEEE 15th Int. Conf. Compat., Power Electron. Power Eng.*, 2021, pp. 1–7.

[5] T. Guillod, P. Papamanolis, and J. W. Kolar, "Artificial neural network (ANN) based fast and accurate inductor modeling and design," *IEEE Open J. Power Electron.*, vol. 1, pp. 284–299, 2020.

[6] H. Komurcugil, S. Biricik, and N. Guler, "Indirect sliding mode control for DC–DC SEPIC converters," *IEEE Trans. Ind. Inform.*, vol. 16, no. 6, pp. 4099–4108, Jun. 2020.

[7] H. Du, C. Jiang, G. Wen, W. Zhu, and Y. Cheng, "Current sharing control for parallel DC–DC buck converters based on finite-time control technique," *IEEE Trans. Ind. Inform.*, vol. 15, no. 4, pp. 2186–2198, Apr. 2019.

[8] S. Lucia, D. Navarro, B. Karg, H. Sarnago, and O. Lucia, "Deep learning-based model predictive control for resonant power converters," *IEEE Trans. Ind. Inform.*, vol. 17, no. 1, pp. 409–420, Jan. 2021.

[9] G. D. Capua and N. Femia, "A novel method to predict the real operation of ferrite inductors with moderate saturation in switching power supply applications," *IEEE Trans. Power Electron.*, vol. 31, no. 3, pp. 2456–2464, Mar. 2016.

[10] M. S. Perdigão, J. P. F. Trovão, J. M. Alonso, and E. S. Saraiva, "Large-signal characterization of power inductors in EV bidirectional DC–DC converters focused on core size optimization," *IEEE Trans. Ind. Electron.*, vol. 62, no. 5, pp. 3042–3051, May 2015.

[11] A. Oliveri, M. Lodi, and M. Storace, "Nonlinear models of power inductors: A survey," *Int. J. Circuit Theory Appl.*, vol. 50, no. 1, pp. 2–34, 2022.

[12] A. Oliveri, G. Di Capua, K. Stoyka, M. Lodi, M. Storace, and N. Femia, "A power-loss-dependent inductance model for ferrite-core power inductors in switch-mode power supplies," *IEEE Trans. Circuits Syst. I: Reg. Papers*, vol. 66, no. 6, pp. 2394–2402, Jun. 2019.

[13] A. Abramovitz and S. Ben-Yaakov, "RGSE-based SPICE model of ferrite core losses," *IEEE Trans. Power Electron.*, vol. 33, no. 4, pp. 2825–2831, Apr. 2018.

[14] X. Duan and A. Q. Huang, "Current-mode variable-frequency control architecture for high-current low-voltage DC–DC converters [letters]," *IEEE Trans. Power Electron.*, vol. 21, no. 4, pp. 1133–1137, Jul. 2006.

[15] W.-H. Yang et al., "A constant-on-time control DC–DC buck converter with the pseudowave tracking technique for regulation accuracy and load transient enhancement," *IEEE Trans. Power Electron.*, vol. 33, no. 7, pp. 6187–6198, Jul. 2018.

[16] G. Vitale, G. Lullo, and D. Scirè, "Thermal stability of a DC/DC converter with inductor in partial saturation," *IEEE Trans. Ind. Electron.*, vol. 68, no. 9, pp. 7985–7995, Sep. 2021.

[17] D. Scirè, G. Lullo, and G. Vitale, "Non-linear inductor models comparison for switched-mode power supplies applications," *Electronics*, vol. 11, no. 15, 2022, Art. no. 2472.

[18] C. W. T. McLyman, *Transformer and Inductor Design Handbook*, 4th ed. Boca Raton, FL, USA: CRC Press, 2011.

[19] A. Van den Bossche and V. C. Valchev, *Inductors and Transformers for Power Electronics*, 1st ed. Boca Raton, FL, USA: CRC Press, 2005.

[20] N. Femia, K. Stoyka, and G. D. Capua, "Impact of inductors saturation on peak-current mode control operation," *IEEE Trans. Power Electron.*, vol. 35, no. 10, pp. 10969–10981, Oct. 2020.

[21] S. Musumeci, L. Solimene, and C. S. Ragusa, "Identification of DC thermal steady-state differential inductance of ferrite power inductors," *Energies*, vol. 14, no. 13, 2021, Art. no. 3854.

[22] A. Oliveri, M. Lodi, and M. Storace, "A piecewise-affine inductance model for inductors working in nonlinear region," in *Proc. 16th Int. Conf. Synth., Model., Anal. Simul. Methods Appl. Circuit Des.*, 2019, pp. 169–172.

[23] P. Burrascano, G. Di Capua, N. Femia, S. Laureti, and M. Ricci, "A pulse compression procedure for power inductors modeling up to moderate nonlinearity," *Integration*, vol. 66, pp. 16–23, 2019.

[24] G. Pilato, G. Vitale, G. Vassallo, and D. Sciré, "Neural modeling of power nonlinear inductors by the E-αNet network," *Nonlinear Dyn.*, vol. 112, no. 19, pp. 17069–17086, 2024.

[25] A. Barili, A. Brambilla, G. Cottafava, and E. Dallago, "A simulation model for the saturable reactor," *IEEE Trans. Ind. Electron.*, vol. 35, no. 2, pp. 301–306, May 1988.

[26] S. F. Roberto, D. Sciré, G. Lullo, and G. Vitale, "Equivalent circuit modelling of ferrite inductors losses," in *Proc. IEEE 4th Int. Forum Res. Technol. Soc. Ind.*, 2018, pp. 1–4.

[27] K. Górecki and K. Detka, "Application of average electrothermal models in the SPICE-aided analysis of boost converters," *IEEE Trans. Ind. Electron.*, vol. 66, no. 4, pp. 2746–2755, Apr. 2019.
[28] F. Bizzarri, M. Lodi, A. Oliveri, A. Brambilla, and M. Storace, "A nonlinear inductance model able to reproduce thermal transient in SMPS simulations," in *Proc. 2019 IEEE Int. Symp. Circuits Syst.*, 2019, pp. 1–5.
[29] D. Scirè, G. Lullo, and G. Vitale, "Assessment of the current for a non-linear power inductor including temperature in DC-DC converters," *Electronics*, vol. 12, no. 3, 2023, Art. no. 579.
[30] D. Scirè, G. Lullo, and G. Vitale, "Design and modeling of an interleaving boost converter with quasi-saturated inductors for electric vehicles," in *Proc. 2020 AEIT Int. Conf. Elect. Electron. Technol. Automot.*, 2020, pp. 1–6.
[31] D. Scirè, S. Rosato, G. Lullo, and G. Vitale, "Characterization of non-linear inductors including thermal effects for power applications," *Renewable Energy Power Qual. J.*, vol. 1, no. 16, pp. 728–734, 2018.
[32] D. Scirè, G. Vitale, M. Ventimiglia, and G. Lullo, "Non-linear inductors characterization in real operating conditions for power density optimization in SMPS," *Energies*, vol. 14, no. 13, 2021, Art. no. 3924.
[33] M. Kachniarz, J. Salach, R. Szewczyk, and A. Bieńkowski, "Temperature influence on the magnetic characteristics of Mn-Zn ferrite materials," in *Progress in Automation, Robotics and Measuring Techniques*, R. Szewczyk, C. Zieliński, and M. Kaliczyńska, Eds. Cham, Switzerland: Springer, 2015, pp. 121–127.
[34] C. Chen et al., "Online inductor parameters identification by small-signal injection for sensorless predictive current controlled boost converter," *IEEE Trans. Ind. Inform.*, vol. 13, no. 4, pp. 1554–1564, Aug. 2017.
[35] M. Ventimiglia, D. Sciré, G. Lullo, and G. Vitale, "A measurement system for power inductors in non-linear operating conditions," in *Proc. IEEE 30th Int. Symp. Ind. Electron.*, 2021, pp. 1–6.

Daniele Scirè (Member, IEEE) was born in Palermo, Italy, in 1991. He received the M.S. degree in electronic engineering and the Ph.D. degree in information and communication technologies from the University of Palermo, Palermo, Italy, in 2017 and 2021 respectively.

From 2018 to 2019, he was a Visiting Ph.D. Student with the Photovoltaic Material and Devices group, Delft University of Technology, Delft, The Netherlands. Since 2022, he has been an Assistant Professor with the University of Palermo. His current research interests include power electronics converter and their control, nonlinear magnetic components, modeling and design of solar cells, and thin film deposition and characterization.

Dr. Scirè was the recipient of the Graduate Student Award from the European Material Research Society in 2019 and the Best Paper Award "Salvatore (Enzo) Piazza" from the Department of Engineering, University of Palermo, in 2022. He is a Reviewer for several journals and conferences.

Giuseppe Lullo (Member, IEEE) was born in Palermo, Italy, in 1965. He received the M.S. (Hons.) and Ph.D. degrees in electronic engineering from the University of Palermo, Palermo, Italy, in 1990 and 1995, respectively.

From 1993 to 1994, he was a Visiting Research Fellow within the Optoelectronics Laboratory, Glasgow University, Glasgow, U.K., and in 1998, a Visiting Scientist within the Department of Electronics and Computer Science, Massachusetts Institute of Technology, Cambridge, MA, USA. In 1999, he became a Researcher and in 2005, an Associate Professor of electronics with the University of Palermo. More recently, he has been involved in research in the field of power electronic systems. He holds a patent on an optical diffractometer. He also founded and comanaged for twenty years, as a Chief Technical Officer, Microtech s.r.l., a high-tech spin-off company devoted to the realization of laser direct writing equipments for microlithographic processes. His research interests include several areas, regarding the design and fabrication of optoelectronic and electronic devices, the design of custom optical systems, the design of mixed-signal electronic systems, and electronics for controlling X-ray satellite telescopes.

Dr. Lullo is a Member of the Italian National Institute for Astrophysics.

Gianpaolo Vitale (Senior Member, IEEE) was born in Palermo, Italy, in 1964. He received the M.S. degree in electronic engineering from the University of Palermo, Palermo, Italy, in 1988.

He is the Research Director with the Institute for High Performance Computing and Networking belonging to the National Research Council of Italy. He teaches "industrial electronics" with the Department of Engineering, MD Electronics Engineering, University of Palermo. He has coauthored two books, two edited books, four book chapters, and more than 100 scientific works. His current research interests include the fields of power electronics, power generation from renewable sources, electromagnetic compatibility, and robotics.

Prof. Vitale is reviewer for several journals and conferences.